Turbulence-driven anisotropic electron tail generation during magnetic reconnection

A. M. DuBois, A. Scherer, A. F. Almagri, J. K. Anderson, M. D. Pandya, and J. S. Sarff

Citation: Physics of Plasmas **25**, 055705 (2018); doi: 10.1063/1.5016240
View online: https://doi.org/10.1063/1.5016240
View Table of Contents: http://aip.scitation.org/toc/php/25/5
Published by the American Institute of Physics

Turbulence-driven anisotropic electron tail generation during magnetic reconnection

A. M. DuBois,[a] A. Scherer, A. F. Almagri, J. K. Anderson, M. D. Pandya, and J. S. Sarff
Department of Physics, University of Wisconsin–Madison, 1150 University Ave., Madison, Wisconsin 53706, USA

(Received 17 November 2017; accepted 11 February 2018; published online 13 March 2018)

Magnetic reconnection (MR) plays an important role in particle transport, energization, and acceleration in space, astrophysical, and laboratory plasmas. In the Madison Symmetric Torus reversed field pinch, discrete MR events release large amounts of energy from the equilibrium magnetic field, a fraction of which is transferred to electrons and ions. Previous experiments revealed an anisotropic electron tail that favors the perpendicular direction and is symmetric in the parallel. New profile measurements of x-ray emission show that the tail distribution is localized near the magnetic axis, consistent modeling of the bremsstrahlung emission. The tail appears first near the magnetic axis and then spreads radially, and the dynamics in the anisotropy and diffusion are discussed. The data presented imply that the electron tail formation likely results from a turbulent wave-particle interaction and provides evidence that high energy electrons are escaping the core-localized region through pitch angle scattering into the parallel direction, followed by stochastic parallel transport to the plasma edge. New measurements also show a strong correlation between high energy x-ray measurements and tearing mode dynamics, suggesting that the coupling between core and edge tearing modes is essential for energetic electron tail formation. *Published by AIP Publishing.*
https://doi.org/10.1063/1.5016240

I. INTRODUCTION

Magnetic reconnection (MR) is characterized by impulsive, discrete bursts of released magnetic energy (U_{mag}). The release of U_{mag} and conversion to kinetic energy plays an important role in particle transport and energization (heating and acceleration) in space and laboratory plasmas. An ongoing topic of research is the underlying mechanism behind particle heating and energization during magnetic reconnection. Electron energization during MR is commonly observed in the magnetotail,[1–3] during magnetospheric substorms,[4,5] and during solar flares[6,7] during MR events. However, space-based observations and *in situ* measurements are challenging to obtain due to the uncertainty in both the location and the time of MR.

MR is also prevalent in laboratory experiments,[8–15] particularly in tokamaks where electron energization is commonly observed during the internal kink mode sawtooth cycle. X-ray detectors have become increasingly useful diagnostics for diagnosing electron dynamics in high temperature plasma[16–23] experiments. Parallel and anti-parallel anisotropy in x-ray emission from non-thermal electrons, attributed to runaway acceleration driven by the inductive electric field created during the impulsive sawtooth crash, has been measured in the T-10[18], VTF,[8] TCV,[9] and PLT[11] tokamaks. In the reversed field pinch (RFP), discrete MR events resemble the internal kind mode sawteeth and release large amounts of energy from the equilibrium magnetic field, a large fraction of which is transferred to the ions in a non-collisional process. The extensive diagnostic set available on the Madison Symmetric Torus (MST) offers a unique opportunity to study particle heating and energization processes more in depth in a controlled and reproducible laboratory setting.

Ion heating and energization has been thoroughly studied[24–30] in MST RFP plasmas, but emphasis has recently shifted toward understanding transient electrons during bursts of MR. High-speed x-ray energy spectrum measurements described in DuBois *et al.*[31] revealed the formation of a non-Maxwellian energetic electron tail during MR in standard RFP plasmas in MST. The energetic tail was characterized by a power-law with the spectral index decreasing at MR, and then increasing rapidly. The x-ray emission was found to be anisotropic favoring the radial view and symmetric in toroidal views, suggesting a tail generation process that favors a direction perpendicular to the magnetic field. This also implied that runaway acceleration was not the responsible mechanism, consistent with the net emf acting on electrons being smaller than the Dreicer field. Modeling of the bremsstrahlung emission was consistent with the generation of an anisotropic electron tail having high perpendicular velocity and predicted the extent of the electron tail to be spatially localized near the magnetic axis. It was predicted that a turbulent process related to tearing fluctuations was most likely responsible for the energization observed in the electron tail. This was the first experimental evidence of anisotropic electron energization during MR in a toroidal, magnetically confined plasma that favored a direction perpendicular to the magnetic field.

These previous results motivated further experiments, which aimed to make a direct measurement of the radial extent of the core-localized tail, make estimates of the onset time of energization, and uncover the energy source and

Note: Paper NI2 4, Bull. Am. Phys. Soc. **62**, 209 (2017).
[a]Invited speaker.

mechanism for the electron energization. These new results form the basis of the paper. The MST and MR due to tearing mode instabilities are described in Sec. II. An overview of the fast x-ray (FXR) detector system[32] used for measurements of bremsstrahlung emission during MR is presented in Sec. III, followed by a summary of previous ion heating and energization measurements and a review of the previous electron energization results. New measurements of the core-localized tail radial profile and a discussion on the correlation between tearing dynamics and electron energization are presented in Sec. IV.

II. THE MADISON SYMMETRIC TORUS

MST is a toroidal device with a 1.5 m major radius and a 0.52 m minor radius where the plasma is surrounded by a 5-cm-thick aluminum conducting shell.[33] MST is typically operated in a RFP configuration where the magnetic field is generated primarily by current in the plasma. MST can operate with a plasma current (I_p) between 200 and 600 kA, which corresponds to a magnetic field strength of 0.2 to 0.6 T in the core. The line-averaged electron density $\sim 10^{19}$ m^{-3}, and core electron and ion temperatures are between 0.2 and 2 keV. The typical pulse has a 10 ms I_p ramp up period followed by a 20–30 ms long flat-top and an overall pulse length <100 ms. Plasmas in the standard confinement regime have an energy confinement time of a few ms, while the energy confinement in the reduced-tearing regime is much larger, about 10 ms.

The work described here is for plasmas in the standard confinement regime, which exhibit strong, quasiperiodic MR events associated with tearing instabilities. Magnetic reconnection arises from tearing modes that are destabilized by the gradient of the parallel current density. This is associated with the strong toroidal induction and ohmic heating that forms the plasma. Tearing mode resonances can occur at many locations in the plasma volume at radial locations where the safety factor, $q(r) = m/n$ (m = poloidal mode number, n = toroidal mode number) due to the strong magnetic shear in the RFP equilibrium. Typically, a few tearing modes resonant in the core region are linearly unstable, which have mode numbers $m = 1$, $n = 6$–8. Stable $m = 1$ modes with $n > 8$ are nonlinearly excited in the mid-region of plasma as well as at the $q(r) = 0$ surface where $m = 0$ modes are resonant. The toroidal magnetic field crosses zero at the $q(r) = 0$ surface and reverses direction near the boundary. The reversal surface location can be controlled and even completely removed from the plasma, and this strongly affects the nonlinear dynamics of MR associated with the coupling of $m = 1$ and $m = 0$ modes. The degree of toroidal field reversal is quantified by the reversal parameter, $F = B_t(a)/\langle B_t \rangle$, where $B_t(a)$ is the toroidal magnetic field at the wall and $\langle B_t \rangle$ is the average toroidal magnetic field in the whole plasma volume. As F becomes more negative, the reversal surface is moved inward toward the core. For $F = 0$, the reversal surface is located at the wall of the conducting shell and all of the toroidal flux is generated by current in the plasma.

The nonlinear interaction between tearing modes results in MR being excited at many sites that conspire to create a quasiperiodic magnetic relaxation cycle that causes a sudden release of stored magnetic energy, U_{mag}, during a fast ($\sim$100 μs) crash phase.[34] This cycle resembles the internal kink mode sawtooth process in tokamak plasmas in some respects, but it is more global in RFP plasmas due to its multi-mode nature. The overlap of magnetic islands from multiple tearing modes leads to widespread magnetic stochasticity, enhancing parallel particle and energy transport.[35–37] Figure 1 shows two typical magnetic relaxation cycles during a single discharge in MST. Figure 1(a) shows U_{mag} during a 10 ms window. The magnetic fluctuation amplitudes for an unstable core-resonant $m = 1$, $n = 6$ mode (blue, dashed) and a nonlinearly driven edge-resonant $m = 0$, $n = 1$ mode (red, solid) are shown in Fig. 1(b). Figure 1(c) shows an example of the reversal parameter, where the minimum F reached during MR is dependent on the individual event and not the set-point of F. The insets in Fig. 1 show the evolution (relative to MR) of U_{mag} (top) and magnetic fluctuation amplitudes (bottom) averaged over 485 MR events. At the MR event, 20–30 kJ of U_{mag} is released in 100 μs, and both core and edge-resonant mode amplitudes peak. Analysis of time resolved x-ray data in this paper is based on conditional averaging where the time of the MR event is set to zero and all data are gathered in a window centered around the time of MR and ranging from 1 ms before to 1 ms after. These time windows are selected during the flattop of the discharge between 10 and 30 ms where the plasma current and density are constant and

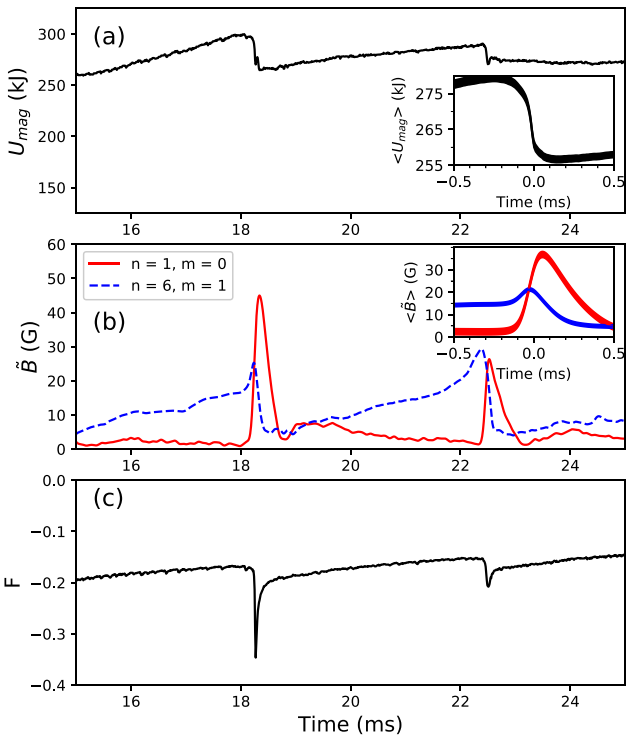

FIG. 1. (a) Evolution of U_{mag} for two magnetic reconnection cycles in a 500 kA standard ($F = -0.2$) plasma in MST. (b) Evolution of tearing mode amplitudes for the edge-resonant $m = 1$, $n = 1$ (red, solid) mode and the (innermost) core resonant $m = 1$, $n = 6$ (blue, dashed) mode. (c) The evolution of the reversal parameter, F. Notice that the minimum F at the MR is dependent on each individual event. The insets show the magnetic energy (top) and tearing mode amplitudes (middle) averaged over 485 events (shaded region represents the standard error of the mean), with time relative to MR.

within a pre-specified range. Only MR events that generate a change in toroidal magnetic flux characterized by a one-turn poloidal voltage above 12 V are considered, and all of the selected MR events are then averaged together to characterize dynamical changes in the data.

III. FAST X-RAY DETECTOR DIAGNOSTIC

The fast x-ray (FXR) detector[32] is a high-time resolution soft x-ray spectrometer that measures electron energization via emitted bremsstrahlung and is installed on MST for MR studies. The detector consists of a PerkinElmer Inc., Si-APD (Silicon Avalanche PhotoDiode) type C30703F with a 10 mm × 10 mm active area. A high voltage power supply is used to apply a bias of +430 V to the APD. The APD output signal is proportional to the energy of the incident photon and is input to a Gaussian amplifier with a shaping time of 20 ns. The shaping amplifier increases the magnitude of the signal which increases signal to noise ratio. The full width at half maximum (FWHM) of each Gaussian pulse is ∼20 ns, allowing for high time resolution measurements. The amplified signal is digitized at a rate of 500 MHz using a ZT410PXI-21 ZTec digitizer with a 14-bit sampling resolution. A radioactive iron source (Fe55) with a strong line at 5.9 keV is used to calibrate the FXR detector system and derive a characteristic pulse as well as a range of acceptable FWHM values that are later used in experimental data to determine if the signal is generated by an x-ray pulse or noise. The pulse height analysis (PHA) of calibration data yields a detector optimal energy range of 2–30 keV and an energy resolution of 1.0 keV. Figure 2 shows a typical x-ray pulse from the Fe55 source (black) with the characteristic pulse (red) fitted to the data. The blue dashed line shows a spline fit to the data, which is used to calculate the FWHM of the pulse (17.3 ns). The energy of the pulse is 5.8 keV.

PHA of experimental data is used to discriminate between noise and x-ray photons based on the shape and the FWHM of the pulse. If the pulse is verified to be from an x-ray, the time relative to MR and the energy of the pulse is recorded. To calculate an energy spectrum, a series of similar discharges is taken, and all x-ray pulses are counted and separated into a range of energy bins for the full ensemble of shots. To calculate the total x-ray flux in plasma, raw x-ray counts are corrected by detector efficiency, time window (20 μs), and energy resolution (1.0 keV). The detector efficiency is dependent on the probability of transmission through a number of materials and the probability of a photon interacting with the silicon detector. Total x-ray flux can be normalized by plasma core volume through which the detector views and the number of MR events.

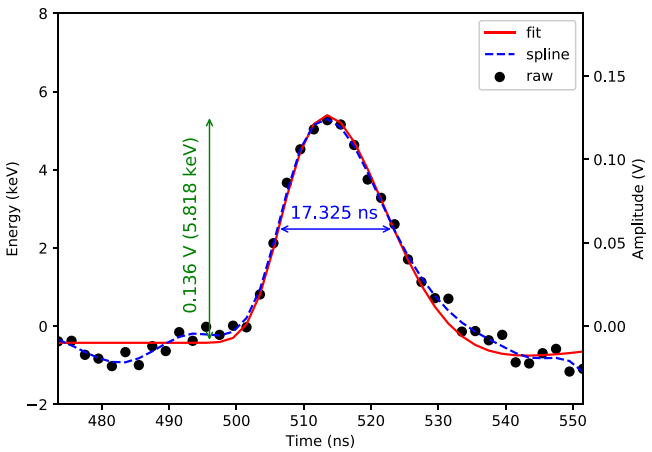

FIG. 2. A single Fe55 photon pulse (black) measured by the FXR detector with a characteristic pulse fit (red) and the spline fit (dashed, blue). The best-fit amplitude is 5.818 keV with a full width at half maximum, as calculated from the spline fit, of 17.325 ns.

The detector has the versatility to be quickly moved for measurements through chords viewing different impact parameters and directions relative to the guide magnetic field. In the experiments described below, the FXR detector is switched between two different views, a radial [Fig. 3(a), blue] and a toroidal view [Fig. 3(a), black]. The radial view has a radial line of sight along a minor radial chord with an angular acceptance of ∼15° that perpendicularly intersects the magnetic axis. The toroidal view has an angle of acceptance of ∼5° located just below the mid-plane and centered along the magnetic axis. In addition to these two views, MST has a set of 13 chordal views that cover the plasma minor cross section. These 13 parallel chords, shown in Fig. 3(b), have 10 cm spacing and cover about 70% of the core region. The FXR detector was placed on the chords in red for line averaged profile measurements. There is a molybdenum limiter associated with an unused rf antenna mounted on the inner wall of the vessel that is located in the line-of-sight of the innermost chord [Fig. 3(b), far left], which creates target emission contamination in that view. Each x-ray detector port is fitted with a 150 μm beryllium (Be) window that separates the detector from vacuum and filters out photons with energies less than 2 keV. Additionally, a 5 cm column of air at standard temperature and pressure also limits the low energy cutoff to 2 keV.

IV. EXPERIMENTAL RESULTS

A. Summary of ion heating and energization

Majority and minority (impurity) ion heating and energization has been thoroughly studied on MST, and it is useful for reference to briefly summarize key observations. The earliest ion temperature measurements[24] on MST showed that the ions are rapidly heated by a non-collisional mechanism on a short time scale (∼100 μs) compared to the i-e collision time (∼10 ms). The ion temperature (T_i) can exceed the electron temperature (T_e) during MR. More recent studies have focused on detailed characterization of the heating mechanism(s). The ion heating is significantly diminished when the nonlinear coupling between tearing modes is weakened and the amount of energy released from the equilibrium magnetic field is decreased.[29,30] This confirmed that a large fraction of the released magnetic energy is transferred to the ions and manifest as heating and tail generation. Impurity ion species are also observed to be heated to a higher temperature than the bulk/majority ions.[30] Heating of both majority and minority ions is dependent on ion mass and charge so that heavier ion species are heated more strongly.[27] The cooling time scale is longer than the heating time scale and the global

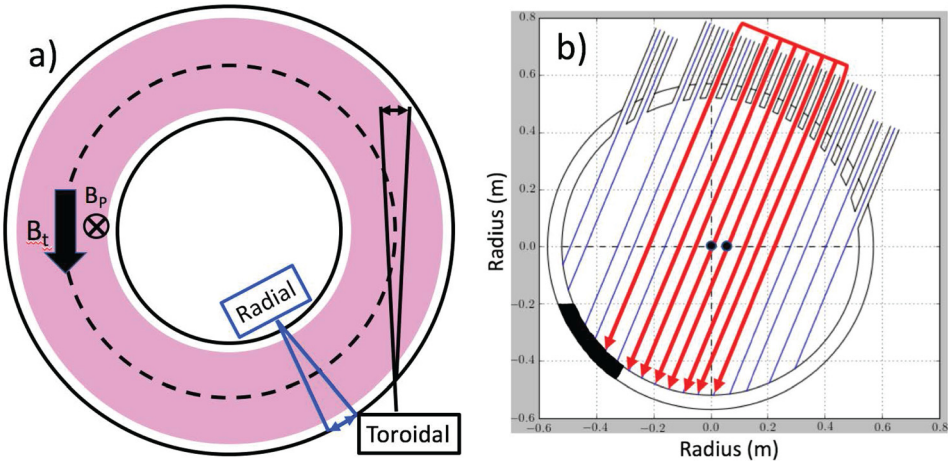

FIG. 3. A schematic of the FXR detector views. (a) The radial view in blue has an angular acceptance of 15° and perpendicularly intersects the magnetic axis. The toroidal (parallel, anti-parallel) view in black has an angular acceptance of 5° and is located just below the midplane and centered on the magnetic axis. (b) The set of 7 parallel chords (red) that view different impact parameters in the plasma. The black dots on the midplane line (horizontal, dashed) indicate the geometric center (left most) and the magnetic axis (right most). A molybdenum limiter mounted on the inner wall of the vessel is located in the line of sight of the two inboard-most measurement chords. The poloidal extent of this limiter is shaded black.

energy confinement time, implying that ion energy is relatively well confined.

Measurements of the ion energy distribution show that MR results in anisotropic ion heating and the generation of a suprathermal tail distribution.[25] The anisotropy is observed in impurity ions such that the increase of the temperature perpendicular to the magnetic field is much larger than the increase of the temperature parallel to the magnetic field. The anisotropy is observed to increase with increasing density, inconsistent with increased collisions. The suprathermal tail appearing in the majority ion distribution is well described by a power-law. The tail spectral index calculated from the power-law rapidly decreases at the reconnection event, indicative of a high energy ion tail formation.

The most likely mechanisms for the observed ion heating are gyro-resonant heating via a turbulence cascade[38] and stochastic heating.[27] Spontaneous ion tail formation could be, in part, facilitated by the runaway process, since this is observed for 25 keV neutral-beam-sourced ions.[26] This is an active research topic.

B. Previous electron energization results

While strong ion heating and energetic ion tail formation are observed during MR events, Thomson scattering measures a cooling of the thermal electron population.[37,39] This is consistent with the increased stochastic thermal transport, which favors electrons with higher parallel energy and may mask electron perpendicular energization during MR events. The high time resolution FXR diagnostic, described in Sec. III, is used to measure energy-resolved bremsstrahlung emission during MR in MST plasmas to reveal fast electron dynamics.

The first experimental evidence for anisotropic electron energization during MR that favors a direction perpendicular to the guide magnetic field in a toroidal, magnetically confined plasma was previously reported in DuBois *et al.*[31] X-ray bremsstrahlung emission is measured along a radial view (Fig. 3, blue) through the plasma core in plasma discharges with $I_p = 500$ kA, $n_e = 0.8 \times 10^{19}$ m^{-3}, and $F = -0.2$. Figure 4 shows spectra for before (black), during (red), and after (blue) the MR event, with the solid lines showing the power-law ($E^{-\gamma}$) fits. For these spectra, the spectral index in the radial view ($\gamma_\perp$) decreases from 4.15±0.03 to 2.15±0.05 during MR, indicating significant flattening of the high energy tail. After the MR event, $\gamma_\perp$ increases to 6.77±0.09, indicating that the nonthermal electrons are lost from the plasma, possibly due to pitch angle scattering. Figure 5 shows the time evolution of $\gamma_\perp$ in 20 μs intervals. Before the MR event, $\gamma_\perp$ is constant, but begins decreasing at t = −44.9 ± 1.0 μs, roughly 175 μs after the magnetic energy begins to decrease. $\gamma_\perp$ reaches a minimum at t = 0 μs before it starts to increase indicating a loss in high energy x-ray flux. As was shown previously,[31] experiments with the FXR detector located on a toroidal view port shows symmetry in the parallel and anti-parallel directions, consistent with low effective parallel electric field during MR events, $\eta J_\parallel / E_D \approx 0.12$ where E_D is the Dreicer[40] field.

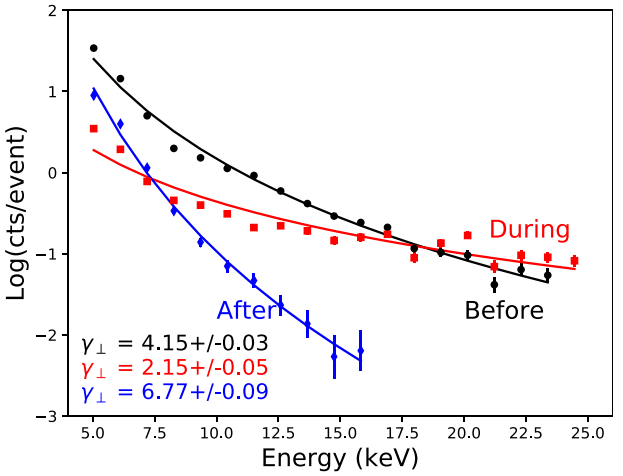

FIG. 4. X-ray energy spectra measured in the radial view for 20 μs windows 0.5 ms before (black), during (red) and 0.5 ms after (blue) MR. Each spectrum is fit with a power-law (solid lines), from which $\gamma_\perp$ is calculated.

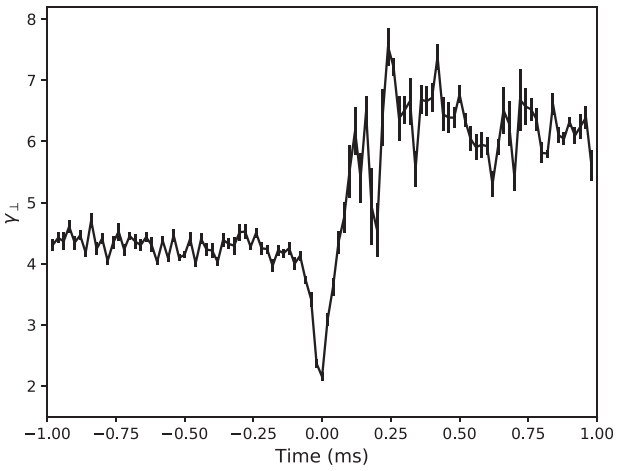

FIG. 5. The $\gamma_\perp$ calculated from power-law fits to the x-ray energy spectra as a function of time relative to MR.

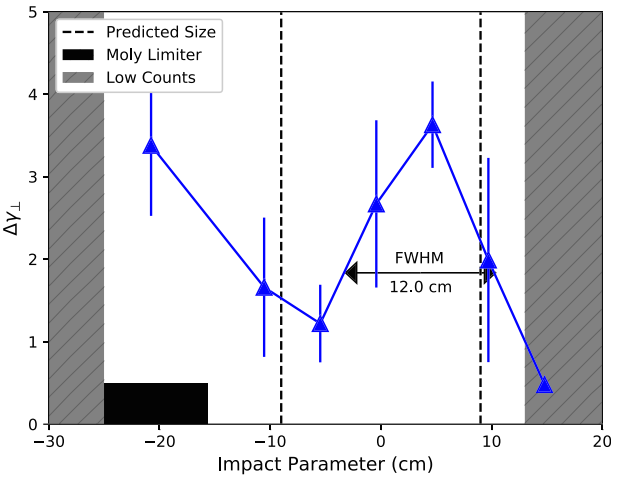

FIG. 6. The $\Delta\gamma_\perp$ as a function of impact parameter relative to the magnetic axis (blue). The vertical lines (dashed, black) show the 9 cm radial extent of the core-localized energetic tail predicted by the CQL3D modeling, and the black bar shows the location of a molybdenum limiter. The gray shaded areas indicate low x-ray photon counts.

The CQL3D code (a relativistic collisional/quasilinear 3D Fokker-Planck solver[41]) was used to model a mock tail having a power-law energy distribution localized in $v_\perp$. The mock tail has a Gaussian radial profile centered on-axis. When the radial extent of the tail is set to 9 cm, the predicted x-ray bremsstrahlung energy spectra along the radial and toroidal lines-of-sight show symmetric toroidal views and strong perpendicular anisotropy for $E > 10$ keV, where the flux is larger in the radial view, consistent with measurements of bremsstrahlung emission during MR in MST plasmas. The tail in the radial view becomes more dominant over the toroidal view as the radial extent of the core region is reduced further. These results motivated the present experiments, described in Sec. IV C, to quantify the radial extent of the observed electron tail.

C. Core-localized tail radial profile

In the following set of measurements, data were taken in plasma discharges with $I_p = 500$ kA, $n_e = 0.8 \times 10^{19}$ m^{-3}, and $F = -0.2$. The set of vertical viewing chords shown in Fig. 3(b) allows for a direct measurement of the radial extent of the core-localized energetic electron tail, which can then be compared with the CQL3D modeling described in Sec. IV B. The FXR detector was mounted on 7 chordal views [Fig. 3(b), red] that have different impact parameters relative to the magnetic axis (6 cm outboard from the geometric center), all on the same toroidal plane, to make a measurement of the line-of-sight x-ray energy spectrum as a function of the impact parameter. The energy spectra are used to calculate the change in the spectral index from before MR compared to during the MR event, $\Delta\gamma_\perp$. Figure 6 shows $\Delta\gamma_\perp$ as a function of impact parameter relative to the magnetic axis (blue). The dashed line shows the 9 cm radial extent of the core-localized electron tail assumed in the CQL3D modeling described in Sec. IV B. The $\Delta\gamma_\perp$ profile is fitted to a Gaussian with a FWHM of $\sim$12 cm, or a radial extent of 6 cm. This Gaussian profile of the core-localized tail lies within and is slightly narrower than the size assumed in the CQL3D modeling. The black bar indicates the span of an existing Moly limiter that happens to be mounted on the vessel wall and is viewed by the innermost chord. This chord serves as an indicator of the time delay from when a high energy electron from the core region reaches the edge where the Moly limiter is located. However, the x-ray flux from this chord (between -15 cm and -30 cm) is contaminated due to target emission produced by the limiter. Note that the outermost chords in Fig. 3(b) (black lines) are located near the reversal surface where the mean magnetic field is in the poloidal direction. These chords (represented by the gray shaded regions in Fig. 6) are far from the plasma core, where the plasma temperature is much lower, and as a result the high-energy x-ray photon count rate is insufficient to gather enough statistics to calculate an energy spectrum.

It was seen previously that the duration of tail formation is shorter for the toroidal views than for the radial view. This is quantified by a Gaussian curve fit to $\gamma(t)$ centered on $t = 0$ ms. The temporal FWHM is a measure of how long these energetic electrons survive before they are no longer in the detector line-of-sight. Figure 7 shows the FWHM (blue) of the Gaussian fits for the vertical chords, with the error bars taken from the covariance matrix of each γ Gaussian fit. In the region of the core-localized tail, the FWHM calculated for each chord is larger than for the previous measurement of 30.1 ± 0.9 μs for $\gamma_\parallel$. The peak of the profile is at $r = 4.7$ cm near the magnetic axis, which also coincides with the location of the maximum $\Delta\gamma_\perp$. Moving radially inboard and outboard from the core, the FWHM decreases to values that are comparable to the FWHM estimated for the toroidal view. This shows that the duration of the energization process is longest near the magnetic axis and that energetic electrons are lost from the detector line-of-sight faster near the edge of the core-localized region than near the magnetic axis.

It is also possible to estimate the onset of energization, or the time at which γ decreases below a stipulated threshold, from the temporal Gaussian fits to $\gamma(t)$. This threshold is selected to be 20% of the minimum γ. The previous data for $\gamma_\perp$ and $\gamma_\parallel$ in DuBois *et al.*[31] indicated that there is a delay in the decrease in the toroidal view. The more comprehensive

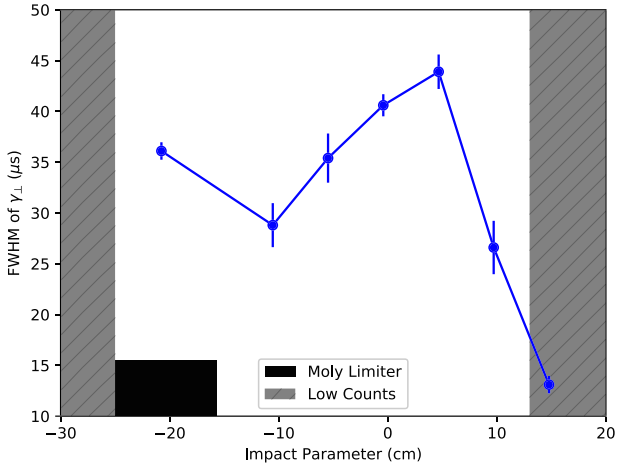

FIG. 7. A radial profile of the FWHM of γ around the time of MR is shown in blue. The black bar shows the location of a molybdenum limiter. The gray shaded areas indicate low x-ray photon counts.

data reported here indicate that the decrease in $\gamma_\parallel$ occurs at $t = -22.8 \pm 0.9$ μs, a delay of 22.1 μs relative to $\gamma_\perp$, which begins decreasing at $t = -44.9 \pm 1.0$ μs. This suggests that energetic electrons with high parallel energy are created 22.1 μs after energetic electrons with high perpendicular energy are generated. This also indicates that the energization process favors the perpendicular direction, with pitch angle scattering into the parallel direction where the appearance of a high energy tail is delayed. The relatively slow Coulomb collisional process for higher energy electrons (e.g., $\nu \sim 200\,s^{-1}$ at 20 keV) also supports the hypothesis that turbulent scattering might be an important contributor in pitch angle diffusion. Previous data also indicated that $\gamma_\parallel$ relaxes faster than $\gamma_\perp$ following MR, indicating that relatively rapid parallel transport is taking place.

The duration of energization measured at the different impact parameters also reveals the time scale that fast electrons escape the 6 cm radius core region. The onset time of energization is plotted for each vertical chord in Fig. 8 (blue).

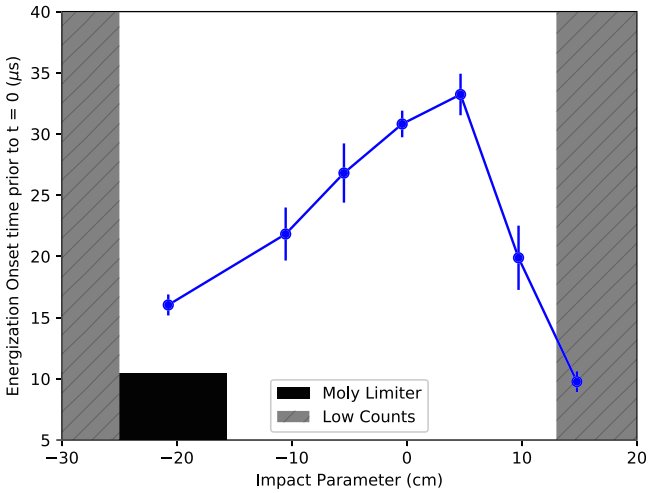

FIG. 8. A radial profile of the energization onset time (before MR) is shown in blue. This onset time indicates when an energetic tail begins to form. The black bar shows the location of a molybdenum limiter. The gray shaded areas indicate low x-ray photon counts.

The profile in Fig. 8 shows that in the region of the core-localized energetic electron tail, the energization begins at $t = -33.2 \pm 1.7$ μs, approximately 187 μs after the initial decrease in U_{mag}. The earlier onset time (peak of the radial profile in Fig. 8) is localized near the magnetic axis and the onset time becomes later moving radially away from the magnetic axis. At the edge of the core-localized region ($r = |10|$ cm), energization arises at $t = -21.8 \pm 2.2$ μs (inboard) and -19.9 ± 2.6 μs (outboard), consistent with the toroidal view dynamics. This indicates that fast electrons are initially observed 10.4 μs later in the toroidal view and at the edge of the core-localized region than near the magnetic axis. Outside of the core-localized region ($r > |10|$ cm), the energization activates at $t = -16.0 \pm 0.9$ μs for the chord viewing the Moly limiter, which is 6.8 μs later than the onset of energetic electrons in the toroidal view.

This may reveal the radial diffusion of high energy electrons that travel $\Delta r \approx 50$ cm in $\Delta t \approx 17.2$ μs. Given these quantities, the radial diffusion rate for an electron with energies between 10 and 20 keV is estimated to be 14 500 m^2/s. For standard RFP plasmas, where the radial diffusion rate for thermal electrons (here ~500 eV) in the core region can be as large as 1000 m^2/s,[36] the estimated diffusion rate for energetic electrons is consistent with stochastic transport, $D \sim v_{the} D_{st}$. Note that although the FWHM of γ in the chord viewing the Moly limiter is longer than in the toroidal view, the onset takes place after energetic electrons are initially observed in the toroidal view, consistent with fast electrons being transported to the edge.

D. Correlation with tearing dynamics

The change in the stored U_{mag} and the strength of the MR event tend to be stronger for lower plasma density, higher plasma current, and deeper reversal parameter. In experiments studying ion energization, it was found that the energy source was the released magnetic energy during MR. Additionally, the ion heating mechanism is non-collisional because the observed heating time (μs time scale) is much faster than the i-e collision time ($\tau > 0.01$ s) as well as the fact that bulk electrons are cooled during MR. To assess the scaling of the energy source and isolate the mechanism behind the observed electron energization, x-ray emission in the radial view [Fig. 3(a), blue] is measured in a variety of plasma discharges with plasma current $I_p = 300$–500 kA, electron density $n_e = 0.4$–$1.5 \times 10^{19}\,m^{-3}$, and reversal parameter $F = 0$ to -0.4. Figure 9 shows the $\Delta\gamma_\perp$ as a function of the released magnetic energy, $\Delta U_{mag} = U_{mag-before} - U_{mag-during}$. $\Delta\gamma_\perp$ increases monotonically from 1.94 for $\Delta U_{mag} \sim 15$ kJ to 2.73 for $\Delta U_{mag} \sim 55$ kJ, which implies that the electron tail generated during MR is correlated with the amount of released magnetic energy, similar to what is observed during ion energization.[29,30]

Although the released magnetic energy is the source of electron and ion energization during MR events, the exact mechanism is still unknown. To help shed some light on the underlying mechanism, the tearing mode dynamics are varied by adjusting the plasma equilibrium. In these experiments, the average reversal parameter (averaged over the flattop time between 10 and 30 ms), F_{avg}, is varied to adjust

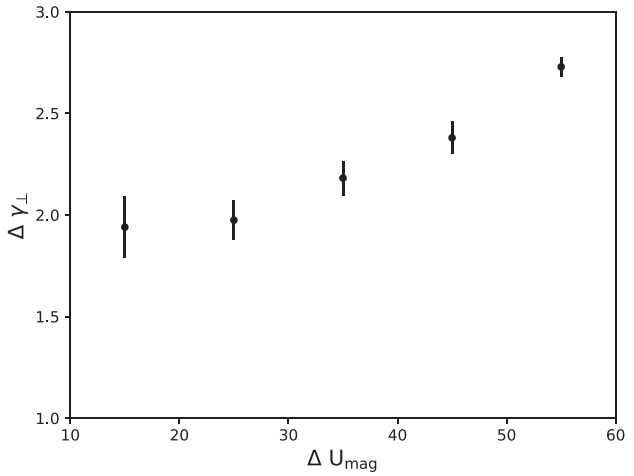

FIG. 9. The change in the spectral index ($\Delta\gamma_\perp$) calculated from x-ray energy spectra measured from the radial view for different amounts of released magnetic energy (ΔU_{mag}) during MR.

the location of the toroidal magnetic field reversal as described in Sec. II. The $m=0$, $n=1$ tearing modes, which are resonant at the reversal surface, facilitate core to edge communication. With deeper reversal ($F<0$), the coupling between edge and core tearing modes is increased. Figure 10 shows $\gamma_\perp$ as a function of time for two reversal parameters: $F_{avg}=0$ (black) and $F_{avg}=-0.3$ (blue). The inset in Fig. 10 shows the average amplitude for the edge $m=0$, $n=1$ tearing mode as a function of time relative to the reconnection event for each discharge. When $F=0$, the $m=0$ mode is nearly removed from the plasma ($\tilde{B}_0 < 10$ G), resulting in a muted ΔU_{mag} and reduced $\Delta\gamma_\perp$. This is consistent with the measurement of greatly reduced high energy x-ray flux. For $F_{avg}=-0.3$, the $m=0$ mode amplitude is 40 G, $\Delta U_{mag}=50$ kJ, and $\Delta\gamma_\perp=2.7$, indicating substantial energetic tail generation, resulting in a significant increase in high energy x-ray flux. The amplitudes of the $m=1$ mode are comparable for both discharges, indicating that the m = 1 modes do not play a direct role despite being part of the nonlinear coupling process. These results demonstrate that electron energization is highly dependent on the coupling between edge and core tearing modes, as was previously shown to be true for ion heating,[29,30] and suggests a turbulent mechanism is similarly active for electron tail energization. However, the precise mechanism is still not known and could be different for electrons and ions.

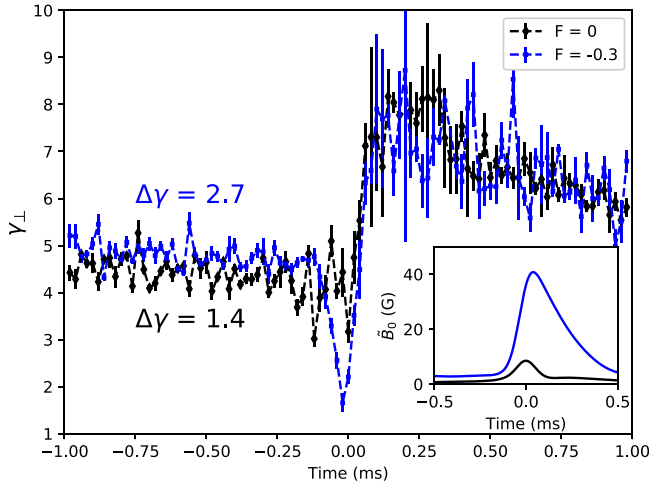

FIG. 10. The time evolution of γ for two reversal parameters: $F=0$ (black) and $F=-0.3$ (blue). The inset shows the average amplitude for the edge $m=0$, $n=1$ tearing mode as a function of time relative to MR for each reversal parameter.

As stated earlier, MR events tend to be stronger for lower plasma density. This was corroborated in ion energization studies,[25] where low density yielded more ion energization and high density amounted to limited energetic tail production. The same is also true for the impurity ion temperature as measured by charge exchange emission.[25] For the density studies described here, x-ray emission is measured in plasmas with $F=-0.2$ and $I_p=500$ kA. The $\gamma_\perp$ is calculated for plasmas with $n_e=0.8\times10^{19}\,\mathrm{m}^{-3}$ (low density) and $n_e=1.2\times10^{19}\,\mathrm{m}^{-3}$ (high density). Figure 11 shows $\gamma_\perp$ as a function of time for low (blue) and high (red) density. Prior to the MR event, $\gamma_\perp$ is already significantly larger (less energetic tail developed) for high density compared to low density, but in both regimes, $\gamma_\perp$ is constant before the MR event. This indicates that even before MR, there is higher percentage of energetic electrons for low density than for high density. Another important feature is that $\gamma_\perp$ begins increasing for high densities before MR (t $\sim$ 0.25 ms). These results show that low density is essential for electron energization during MR events.

A more thorough investigation into the dependence of electron energization on F and the subsequent coupling between edge and core tearing modes can be accomplished by closely examining the minimum reversal parameter (F_{min}) reached during each MR event. Depending on the strength of MR, F_{min} can become more negative, such that the reversal surface moves inward toward the core during MR resulting in more communication between the edge and core. In addition, a more negative F_{min} also leads to more magnetic energy released from the equilibrium magnetic field. F_{min} cannot be directly controlled but can be varied by changing density, reversal parameter, and plasma current. X-ray emission in the radial view is measured in a variety of plasma

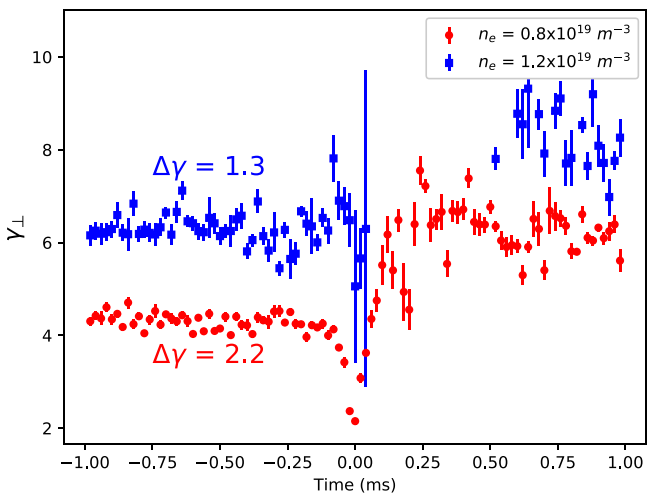

FIG. 11. The evolution of γ for low density (red) and high density (blue) plasmas.

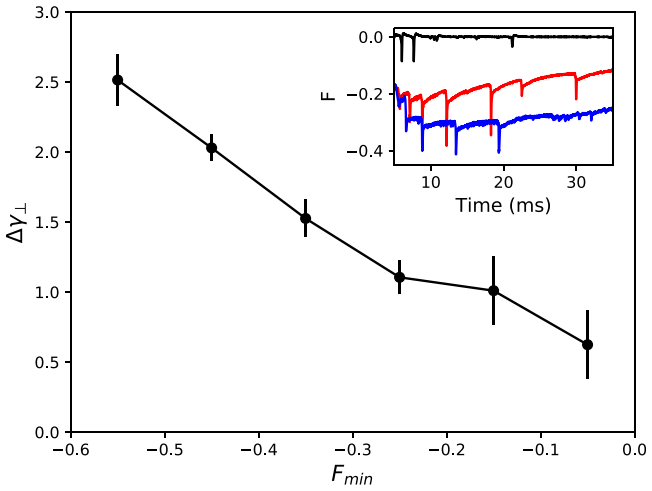

FIG. 12. The $\Delta\gamma_\perp$ as a function of the minimum F achieved during MR (F_{min}). The inset shows three examples of time traces of the reversal parameter, $F = 0$ (black), $F = -0.2$ (red), and $F = -0.3$ (blue).

discharges with $I_p = 300$–$500\,\text{kA}$, $n_e = 0.4$–$1.5 \times 10^{19}\,\text{m}^{-3}$, and $F_{avg} = 0$ to -0.4. Figure 12 shows $\Delta\gamma_\perp$ for a range of F_{min} values, where $\Delta\gamma_\perp$ is linearly dependent on F_{min}. The inset of Fig. 12 shows three examples of time traces of F with set-points of 0 (black), -0.2 (red), and -0.3 (blue), where F_{min} varies depending on the individual MR event.

V. CONCLUSIONS

In previous experiments,[31] high time resolution measurements of x-ray energy spectra provided the first evidence of an anisotropic energetic electron tail arising during MR in a toroidal plasma. CQL3D modeling of a mock electron tail having a power-law energy distribution localized in $v_\perp$ showed that with a 9 cm Gaussian radial extent of the core region centered on axis, the predicted x-ray tail is larger in the radial view than in toroidal views. The tail in the radial view becomes more dominant over the toroidal view as the radial extent of the core region is reduced further. These results led to the motivation to quantify the radial extent of the observed electron tail.

Measurements of the x-ray energy spectra with chordal lines-of-sight through different impact parameters across the plasma on the same toroidal plane confirm that the radial extent of the energetic tail is within 6 cm of the core region, as predicted by CQL3D modeling. The radial profile of the temporal FWHM of γ shows that the peak is localized to the magnetic axis. At the edge of the core-localized region, the FWHM is consistent with measurements in the toroidal view, indicating the amount of time the energization mechanism is active longer near the magnetic axis. The onset of energization appears first in the chord viewing the magnetic axis, roughly 187 μs after magnetic energy is released from the equilibrium magnetic field. The energization onset occurs later in time moving radially away from the magnetic axis, where the onsite time eventually becomes comparable to the toroidal view.

In these experiments, it was verified that the released magnetic energy is the source for the anisotropic electron energization observed during MR, similar to what is observed during ion energization.[29,30] By studying the effect of tearing modes on the electron energization, it was found that increased coupling between edge and core tearing modes is critical for the generation of an energetic tail. This suggests that the anisotropic electron tail formation is due to a turbulent mechanism favoring perpendicular directions. An energetic electron tail is only generated for low density, such that the high collisionality of high density plasmas may hinder more negative f_{min} values necessary to drive increased coupling between tearing modes that is essential for the formation of a high energy electron tail. The delay in the onset of energization between the magnetic axis view, the toroidal view, and the Moly limiter view indicates that the radial diffusion of high energy electrons, which travel $\Delta r \approx 50$ cm in $\Delta t \approx 17.2$ μs, is approximately 14 500 m^2/s, consistent with expectations. This also provides evidence that high energy electrons escape the core-localized region possibly through pitch angle scattering into the parallel direction, followed by stochastic parallel transport to the plasma edge. These results indicate that a similar mechanism is present during MR for both ions and electrons.

SUPPLEMENTARY MATERIAL

See supplementary material for the digital format of the data shown in the figures in this paper.

ACKNOWLEDGMENTS

The authors thank the UW-Madison MST group for the many valuable discussions. This material is based upon work supported by the U.S. Department of Energy Office of Science, Office of Fusion Energy Sciences program under Award No. DE-FC02-05ER54814 and the National Science Foundation under Grant No. PHY08-21899.

[1]M. Hoshino, T. Mukai, T. Terasawa, and I. Shinohara, J. Geophys. Res. **106**, 25979, https://doi.org/10.1029/2001JA900052 (2001).
[2]M. Hoshino, K. Hiraide, and T. Mukai, Earth, Planets Space **53**, 627 (2001).
[3]M. Øieroset, R. P. Lin, T. D. Phan, D. E. Larson, and S. D. Bale, Phys. Rev. Lett. **89**, 195001 (2002).
[4]J. Birn, A. V. Artemyev, D. N. Baker, M. Echim, M. Hoshino, and L. M. Zelenyi, Space Sci. Rev. **173**, 49 (2012).
[5]Q. Pan, M. Ashour-Abdalla, R. J. Walker, and M. El-Alaoui, J. Geophys. Res.: Space Phys. **119**, 1060, https://doi.org/10.1002/2013JA019508 (2014).
[6]R. P. Lin and H. S. Hudson, Sol. Phys. **17**, 412 (1971).
[7]S. Masuda, T. Kosugi, H. Hara, S. Tsuneta, and Y. Ogawara, Nature **371**, 495 (1994).
[8]W. Fox, M. Porkolab, J. Egedal, N. Katz, and A. Le, Phys. Plasmas **17**, 72303 (2010).
[9]I. Klimanov, A. Fasoli, and T. P. Goodman, Plasma Phys. Controlled Fusion **49**, L1 (2007).
[10]P. V. Savrukhin, Phys. Rev. Lett. **86**, 3036 (2001).
[11]S. Von Goeler, J. Stevens, S. Bernabei, M. Bitter, T. K. Chu, P. Efthimion, N. Fisch, W. Hooke, K. Hill, J. Hosea, F. Jobes, C. Karney, J. Mervine, E. Meservey, R. Motley, P. Roney, S. Sesnic, K. Silber, and G. Taylor, Nucl. Fusion **25**, 1515 (1985).
[12]K. Yamasaki, S. Inoue, S. Kamio, T. G. Watanabe, T. Ushiki, X. Guo, T. Sugawara, K. Matsuyama, N. Kawakami, T. Yamada, M. Inomoto, and Y. Ono, Phys. Plasmas **22**, 101202 (2015).
[13]M. Yamada, J. Yoo, J. Jara-Almonte, H. Ji, R. M. Kulsrud, and C. E. Myers, Nat. Commun. **5**, 4774 (2014).
[14]X. Guo, M. Inomoto, T. Sugawara, K. Yamasaki, T. Ushiki, and Y. Ono, Phys. Plasmas **22**, 101201 (2015).

[15]T. Ushiki, M. Inomoto, and H. Koguchi, IEEJ Trans. Fundam. Mater. **134**, 493 (2015).
[16]H. Kawashima and T. Matoba, Rev. Sci. Instrum. **59**, 1816 (1988).
[17]B. Esposito, R. M. Solis, P. Van Belle, O. N. Jarvis, F. B. Marcus, G. Sadler, R. Sanchez, B. Fischer, P. Froissard, J. M. Adams, E. Cecil, and N. Watkins, Plasma Phys. Controlled Fusion **38**, 2035 (1996).
[18]P. V. Savrukhin, Rev. Sci. Instrum. **73**, 4243 (2002).
[19]J. Liptac, R. Parker, V. Tang, Y. Peysson, and J. Decker, Rev. Sci. Instrum. **77**, 103504 (2006).
[20]Y. P. Zhang, Y. Liu, J. W. Yang, X. Y. Song, M. Liao, X. Li, G. L. Yuan, Q. W. Yang, X. R. Duan, and C. H. Pan, Rev. Sci. Instrum. **80**, 126104 (2009).
[21]A. N. James, E. M. Hollmann, and G. R. Tynan, Rev. Sci. Instrum. **81**, 10E306 (2010).
[22]D. J. Clayton, A. F. Almagri, D. R. Burke, C. B. Forest, J. A. Goetz, M. C. Kaufman, and R. O'Connell, Rev. Sci. Instrum. **81**, 10E308 (2010).
[23]J. K. Lepson, P. Beiersdorfer, J. Clementson, M. Bitter, K. W. Hill, R. Kaita, C. H. Skinner, A. L. Roquemore, and G. Zimmer, Rev. Sci. Instrum. **83**, 10D520 (2012).
[24]E. Scime, S. Hokin, N. Mattor, and C. Watts, Phys. Rev. Lett. **68**, 2165 (1992).
[25]R. M. Magee, D. J. Den Hartog, S. T. A. Kumar, A. F. Almagri, B. E. Chapman, G. Fiksel, V. V. Mirnov, E. D. Mezonlin, and J. B. Titus, Phys. Rev. Lett. **107**, 65005 (2011).
[26]S. Eilerman, J. K. Anderson, J. S. Sarff, C. B. Forest, J. A. Reusch, M. D. Nornberg, and J. Kim, Phys. Plasmas **22**, 20702 (2015).
[27]G. Fiksel, A. F. Almagri, B. Chapman, V. Mirnov, Y. Ren, J. Sarff, and P. Terry, Phys. Rev. Lett. **103**, 145002 (2009).
[28]S. T. A. Kumar, A. F. Almagri, D. Craig, D. J. Den Hartog, M. D. Nornberg, J. S. Sarff, and P. W. Terry, Phys. Plasmas **20**, 56501 (2013).
[29]S. Gangadhara, D. Craig, D. A. Ennis, D. J. Den Hartog, G. Fiksel, and S. C. Prager, Phys. Rev. Lett. **98**, 75001 (2007).
[30]S. Gangadhara, D. Craig, D. A. Ennis, D. J. Den Hartog, G. Fiksel, and S. C. Prager, Phys. Plasmas **15**, 056121 (2008).
[31]A. M. DuBois, A. F. Almagri, J. K. Anderson, D. J. Den Hartog, J. D. Lee, and J. S. Sarff, Phys. Rev. Lett. **118**, 75001 (2017).
[32]A. M. DuBois, J. D. Lee, and A. F. Almagri, Rev. Sci. Instrum. **86**, 73512 (2015).
[33]R. N. Dexter, D. W. Kerst, T. W. Lovell, S. C. Prager, and J. C. Sprott, Fusion Technol. **19**, 131 (1991).
[34]J. S. Sarff, A. Almagri, J. K. Anderson, D. L. Brower, D. Craig, B. H. Deng, D. J. Den Hartog, W. X. Ding, G. Fiksel, C. B. Forest, V. Mirnov, S. C. Prager, and V. Svidzinski, in *The Magnetized Plasma in Galaxy Evolution 2004*, edited by K. T. Chyzy, K. Otmianowska-Mazur, M. Soida, and R. J. Dettmar (Observatorium Astronomiczne, Uniwersytet Jagiellonski, Krakow, 2005), pp. 48–55.
[35]S. C. Prager, A. F. Almagri, S. Assadi, J. A. Beckstead, R. N. Dexter, D. J. Den Hartog, G. Chartas, S. A. Hokin, T. W. Lovell, T. D. Rempel, J. S. Sarff, W. Shen, C. W. Spragins, and J. C. Sprott, Phys. Fluids B **2**, 1367 (1990).
[36]T. M. Biewer, C. B. Forest, J. K. Anderson, G. Fiksel, B. Hudson, S. C. Prager, J. S. Sarff, J. C. Wright, D. L. Brower, W. X. Ding, and S. D. Terry, Phys. Rev. Lett. **91**, 45004 (2003).
[37]J. A. Reusch, J. K. Anderson, D. J. Den Hartog, F. Ebrahimi, D. D. Schnack, H. D. Stephens, and C. B. Forest, Phys. Rev. Lett. **107**, 155002 (2011).
[38]V. Tangri, P. W. Terry, and G. Fiksel, Phys. Plasmas **15**, 112501 (2008).
[39]R. M. Magee, *Ion Energization during Tearing Mode Magnetic Reconnection in a High Temperature Plasma* (University of Wisconsin-Madison, 2011).
[40]H. Dreicer, Phys. Rev. **115**, 238 (1959).
[41]R. W. Harvey and M. G. McCoy, in *IAEA TCM on Advances in Sim. and Modelling of Thermonuclear Plasmas, Montreal* (1992), pp. 489–526.